

Submitted to *Astroparticle Physics*

# Constraints on the Geometry of the VHE Emission in LS 5039 from Photon-Photon Deabsorption

Markus Böttcher<sup>1</sup>

## ABSTRACT

Evidence for orbital modulation of the very high energy (VHE)  $\gamma$ -ray emission from the high-mass X-ray binary and microquasar LS 5039 has recently been reported by the HESS collaboration. The observed flux modulation was found to go in tandem with a change in the GeV – TeV spectral shape, which may partially be a result of  $\gamma\gamma$  absorption in the intense radiation field of the massive companion star. However, it was suggested that  $\gamma\gamma$  absorption effects alone can not be the only cause of the observed spectral variability since the flux at  $\sim 200$  GeV, which is near the minimum of the expected  $\gamma\gamma$  absorption trough, remained essentially unchanged between superior and inferior conjunction of the binary system. In this paper, a detailed parameter study of the  $\gamma\gamma$  absorption effects in this system is presented. For a range of plausible locations of the VHE  $\gamma$ -ray emission region and the allowable range of viewing angles, the de-absorbed, intrinsic VHE  $\gamma$ -ray spectra and total VHE photon fluxes and luminosities are calculated and compared to luminosity constraints based on Bondi-Hoyle limited wind accretion onto the compact object in LS 5039. Based on these arguments, it is found that (1) it is impossible to choose the viewing angle and location of the VHE emission region in a way that the intrinsic (deabsorbed) fluxes and spectra in superior and inferior conjunction are identical; consequently, the intrinsic VHE luminosities and spectral shapes must be fundamentally different in different orbital phases, (2) if the VHE luminosity is limited by wind accretion from the companion star and the system is viewed at an inclination angle of  $i \gtrsim 40^\circ$ , the emission is most likely beamed by a larger Doppler factor than inferred from the dynamics of the large-scale radio outflows, (3) the still poorly constrained viewing angle between the line of sight and the jet axis is most likely substantially smaller than the maximum of  $\sim 64^\circ$  inferred from the lack of eclipses. (4) Consequently, the

---

<sup>1</sup>Astrophysical Institute, Department of Physics and Astronomy, Ohio University, Athens, OH 45701, USA

compact object is more likely to be a black hole rather than a neutron star. (5) There is a limited range of allowed configurations for which the expected  $> 1$  TeV neutrino flux would actually anti-correlate with the observed VHE  $\gamma$ -ray emission.

*Subject headings:* gamma-rays: theory — radiation mechanisms: non-thermal — X-rays: binaries — stars: winds, outflows

## 1. Introduction

The recent detections of VHE ( $E \gtrsim 250$  GeV)  $\gamma$ -rays from the high-mass X-ray binary jet sources LS 5039 with the High Energy Stereoscopic System (HESS; Aharonian et al. 2005) and LS I +63°303 with the Major Atmospheric Gamma-Ray Imaging Cherenkov Telescope (MAGIC Albert et al. 2006) establish microquasars as a new class of  $\gamma$ -ray emitting sources. These results confirm the earlier tentative identification of LS 5039 with the EGRET source 3EG J1824-1514 (Paredes et al. 2000) and LSI 61°303 with the COS B source 2CG 135+01 (Gregory & Taylor 1978; Taylor et al. 1992) and the EGRET source 3EG J0241+6103 (Kniffen et al. 1997). Both of these microquasars show evidence for variability of the VHE emission, suggesting an association with the orbital period of the binary system. In the case of LS I +63°303, the association with the orbital period is not yet firmly established since the MAGIC observations covered only a few orbital periods, and the orbital period ( $P = 26.5$  d; Gregory 2002) is very close to the sidereal period of the moon, which also sets a natural windowing period for VHE observations (Albert et al. 2006). In contrast, the HESS observations of LS 5039 provide rather unambiguous evidence for an orbital modulation of both the VHE  $\gamma$ -ray flux and spectral shape with the orbital period of  $P = 3.9$  d (Aharonian et al. 2006). Specifically, Aharonian et al. (2006) found that between inferior conjunction (i.e., the compact object being located in front of the companion star), the VHE  $\gamma$ -ray spectrum could be well fitted with an exponentially cut-off, hard power-law of the form  $\Phi_E \propto E^{-1.85} e^{-E/E_0}$  with a cut-off energy of  $E_0 = 8.7$  TeV. In contrast, the VHE spectrum at superior conjunction is well represented by a pure power-law ( $\Phi_E \propto E^{-2.53}$ ) with a much steeper slope, but identical differential flux at  $E_{\text{norm}} \approx 200$  GeV. The original data from Aharonian et al. (2006), together with these spectral fit functions, are shown in Fig. 1.

A variety of different models for the high-energy emission from high-mass X-ray binaries have been suggested. These range from high-energy processes in neutron star magnetospheres (e.g., Moskalenko et al. 1993; Moskalenko & Karakula 1994; Bednarek 1997, 2000; Chernyakova, Neronov, & Walter 2006; Dubus 2006b), via models with the inner regions of microquasar jets being the primary high-energy emission sites (e.g. Romero et al. 2003; Bosch-Ramon & Paredes 2004; Bosch-Ramon et al. 2005a; Gupta, Böttcher, & Dermer 2006;

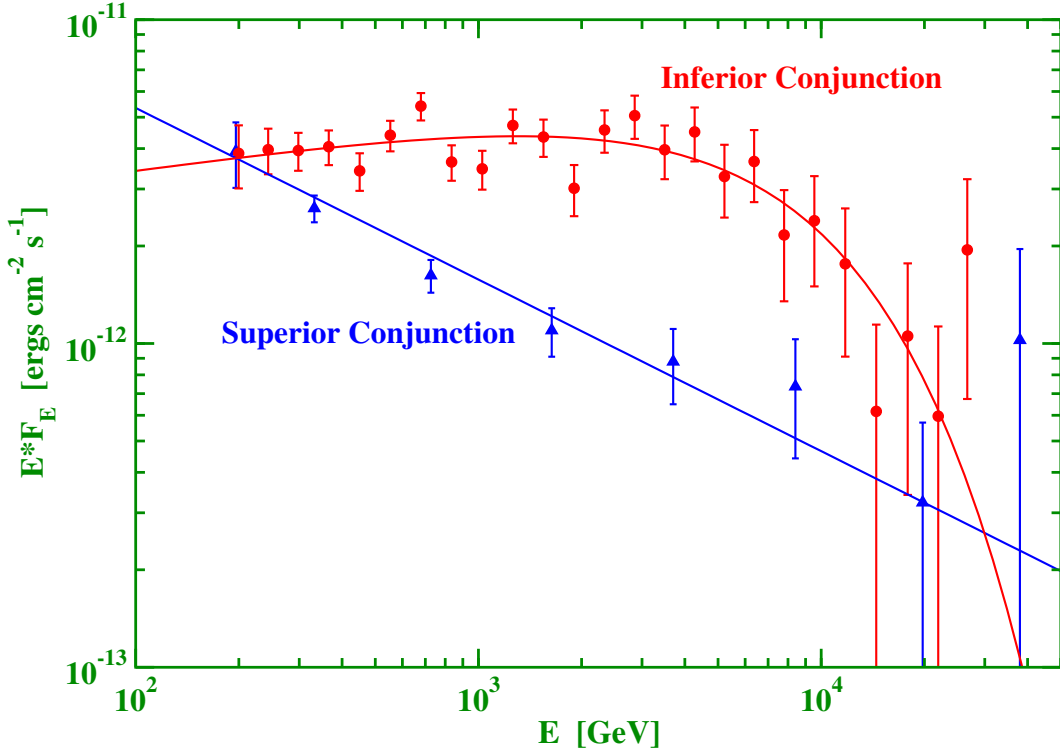


Fig. 1.— VHE  $\gamma$ -ray spectra of LS 5039 around superior (triangles and solid curve) and inferior (circles and dashed curve) conjunction (from Aharonian et al. 2006). The curves indicate the best-fit straight power-law (superior) and exponentially cut-off power-law (inferior) representations of the spectra, on which the analysis in this paper is based.

Dermer & Böttcher 2006; Gupta & Böttcher 2006) and interactions of microquasar jets with the ISM (Bosch-Ramon et al. 2005b), to models involving particle acceleration in shocks produced by colliding stellar winds (e.g., Reimer et al. 2006). In addition to involving a variety of different leptonic and hadronic emission processes, these models also imply vastly different locations of the  $\gamma$ -ray production site with respect to the compact object in LS 5039 and the companion star. However, independent of the emission mechanism responsible for the VHE  $\gamma$ -rays, the intense radiation field of the high-mass (stellar type O6.5V) companion will lead to  $\gamma\gamma$  absorption of VHE  $\gamma$ -rays in the  $\sim 100$  GeV – TeV photon energy range. The characteristic features of the  $\gamma\gamma$  absorption of VHE  $\gamma$ -rays by the companion star light in LS 5039 have been investigated in detail by Böttcher & Dermer (2005) and Dubus (2006a). It was found that, if the  $\gamma$ -ray emission originates within a distance of the order of the orbital separation of the binary system ( $s \sim 2 \times 10^{12}$  cm), this effect should lead to a pronounced  $\gamma\gamma$  absorption trough, in particular near superior conjunction, while  $\gamma\gamma$  absorption tends to be almost negligible near inferior conjunction. In LS 5039, the minimum of the

absorption trough is expected to be located around  $E_{\min} \sim 300$  GeV and should shift from higher to lower energies as orientation of the binary system changes from inferior to superior conjunction.

Most of the relevant parameters of LS 5039, except for the inclination angle  $i$  of the line of sight with respect to the normal to the orbital plane, are rather well determined (see §2). This allows for a detailed parameter study of the  $\gamma\gamma$  absorption effects, leaving the inclination angle and the distance of the VHE emission site from the compact object as free parameters. As will be shown in §3, the effect of electromagnetic cascades will lead to a re-deposition of the absorbed  $\gtrsim 100$  GeV luminosity almost entirely at photon energies  $E \lesssim 100$  GeV. For that reason, one can easily correct for the  $\gamma\gamma$  absorption effect at energies  $E \gtrsim 100$  GeV by multiplying the observed fluxes by a factor  $e^{\tau_{\gamma\gamma}(E)}$  (where  $\tau_{\gamma\gamma}(E)$  is the  $\gamma\gamma$  absorption depth along the line of sight) in order to find the intrinsic, deabsorbed VHE spectra for any given choice of  $i$  and the height  $z_0$  of the VHE  $\gamma$ -ray emission site above the compact object. Results of this procedure will be presented in §4. In §5, these results will then be used to estimate the total flux and luminosity in VHE  $\gamma$ -rays, which can be compared to limits on the available power under the assumption that the VHE emission is powered by Bondi-Hoyle limited wind accretion onto the compact object. This leads to important constraints on the location of the VHE emission site and the geometry of the system, which will be discussed in §6.

## 2. Parameters of the LS 5039 System

LS 5039 is a high-mass X-ray binary in which a compact object is in orbit around an O6.5V type stellar companion with a mass of  $M_* = 23 M_\odot$ , a bolometric luminosity of  $L_* = 10^{5.3} L_\odot \approx 7 \times 10^{38}$  ergs s $^{-1}$  and an effective surface temperature of  $T_{\text{eff}} = 39,000$  °K. The mass function of the system is  $f(M) = (M_{\text{c.o.}} \sin i)^3 / (M_{\text{c.o.}} + M_*)^2 \approx 5 \times 10^{-3} M_\odot$ . The binary orbit has an eccentricity of  $e = 0.35$  and an orbital period of  $P = 3.9$  d. The inclination angle  $i$  is only poorly constrained in the range  $13^\circ \lesssim i \lesssim 64^\circ$ . Under the assumption of co-rotation of the star with the orbital motion, a preferred inclination angle of  $i = 25^\circ$  could be inferred, leading to a compact-object mass of  $M_{\text{c.o.}} = 3.7_{-1.0}^{+1.3} M_\odot$  (Casares et al. 2005). However, since there is no clear evidence for co-rotation, the inclination angle is left as a free parameter in this analysis. Within the entire range of allowed values,  $13^\circ \leq i \leq 64^\circ$ , the mass of the compact object is substantially smaller than the mass of the companion, so that the orbit can very well be approximated by a stationary companion star, orbited by the compact object for our purposes. The orbit has a semimajor axis of length  $a = 2.3 \times 10^{12}$  cm, and the projection of the line of sight onto the orbital plane forms an angle of  $\approx 45^\circ$  with

the semimajor axis (see, e.g., Fig. 4 of Aharonian et al. 2006). Consequently, the orbital separation at superior conjunction is found to be  $s_{\text{s.c.}} = 1.6 \times 10^{12}$  cm, while at inferior conjunction, it is  $s_{\text{i.c.}} = 2.7 \times 10^{12}$  cm.

The mass outflow rate in the stellar wind of the companion has been determined as  $\dot{M}_{\text{wind}} \approx 10^{-6.3} M_{\odot}/\text{yr}$ , and the terminal wind speed is  $v_{\infty} \approx 2500 \text{ km s}^{-1}$  (McSwain & Gies 2002). EVN and MERLIN observations of the radio jets of LS 5039 suggest a mildly relativistic flow speed of  $\beta \sim 0.2$  on the length scale of several hundred AU (Paredes et al. 2002). This would correspond to a bulk Lorentz factor of the flow of  $\Gamma \approx 1.02$ . However, it is plausible to assume that near the base of the jet, where the VHE  $\gamma$ -ray emission may arise (according to some of the currently most actively discussed models), the flow may have a substantially higher speed. Therefore, we will also consider bulk flow speeds of  $\Gamma \sim 2$ , more typical of the jet speeds of other Galactic microquasar jets.

For the analysis in this paper, we use a source distance of  $d = 2.5 \text{ kpc}$ , corresponding to  $4\pi d^2 = 7.1 \times 10^{44} \text{ cm}^2$  (Casares et al. 2005).

Inferred compact object masses and Doppler boosting factors  $D = (\Gamma[1 - \beta \cos i])^{-1}$  for representative values of  $i = 20^\circ$ ,  $40^\circ$ , and  $60^\circ$  and  $\Gamma = 1.02$  and  $\Gamma = 2$  are listed in Table 1.

### 3. The Role of Electromagnetic Cascades

The absorption of VHE  $\gamma$ -ray photons will lead to the production of relativistic electron-positron pairs, which will lose energy via synchrotron radiation and inverse-Compton scattering on starlight photons, and initiate synchrotron or inverse-Compton supported electromagnetic cascades. For photon energies of  $E_{\gamma} \gtrsim 100 \text{ GeV}$ , the produced pairs will have Lorentz factors of  $\gamma \gtrsim 10^5$ . Given the surface temperature of the com-

Table 1. Inferred parameters of the LS 5039 system for three representative values of the inclination angle.

$i$ [ $^\circ$ ]	position	$M_{\text{c.o.}}$ [ $M_{\odot}$ ]	$D(\Gamma = 1.02)$	$D(\Gamma = 2)$	$L_{\text{max}}^{\text{iso}}(\Gamma = 1.02)$ [erg/s]	$L_{\text{max}}^{\text{iso}}(\Gamma = 2)$ [erg/s]
20	i.c.	4.5	1.21	2.68	$6.7 \times 10^{34}$	$1.6 \times 10^{36}$
20	s.c.	4.5	1.21	2.68	$1.9 \times 10^{35}$	$4.6 \times 10^{36}$
40	i.c.	2.3	1.13	1.49	$1.3 \times 10^{34}$	$4.0 \times 10^{34}$
40	s.c.	2.3	1.13	1.49	$3.8 \times 10^{34}$	$1.1 \times 10^{35}$
60	i.c.	1.6	1.09	0.88	$5.6 \times 10^{33}$	$2.4 \times 10^{33}$
60	s.c.	1.6	1.09	0.88	$1.6 \times 10^{34}$	$6.7 \times 10^{33}$

panion star of  $T_{\text{eff}} = 39,000$  K, starlight photons have a characteristic photon energy of  $\epsilon_* \equiv h\nu_*/(m_e c^2) \sim 7 \approx 10^{-6}$ , electrons and positrons with energies of  $\gamma \gtrsim 1/\epsilon_* \sim 1.5 \times 10^5$  will interact with these star light photons in the Klein-Nishina limit and, thus, very inefficiently.  $\gamma$ -rays produced through upscattering of star light photons by secondary electrons and positrons in the Thomson regime will have energies of  $E_{\text{IC}} \lesssim E_{\text{IC}}^{\text{max}} \equiv m_e c^2/\epsilon_* \sim 75$  GeV.

In addition to Compton scattering, secondary electron-positron pairs will suffer synchrotron losses. Magnetic fields even near the base of microquasar jets are unlikely to exceed  $B \sim 10^3$  G. Consequently, along essentially the entire trajectory of VHE photons one may safely assume  $B \equiv 10^3 B_3$  G with  $B_3 \lesssim 1$ . Secondary electrons and positrons traveling through such magnetic fields will produce synchrotron photons of characteristic energies  $E_{\text{sy}} \sim 1.2 \times B_3 \gamma_6^2$  GeV, where  $\gamma_6 = \gamma/10^6$  parametrizes the secondary electron's/positron's energy. Thus, even for extreme magnetic-field values of  $B = 10^3$  G, synchrotron photons at energies  $\gtrsim 100$  GeV could only be produced by secondary pairs with  $\gamma \gtrsim 10^7$ , resulting from primary  $\gamma$ -ray photons of  $E_\gamma \gtrsim 10$  TeV, where only a negligible portion of the total luminosity from LS 5039 is expected to be liberated. Consequently, electromagnetic cascades initiated by the secondary electrons and positrons from  $\gamma\gamma$  absorption in the stellar photon field will re-emit the absorbed VHE  $\gamma$ -ray photon energy essentially entirely at photon energies  $\lesssim 100$  GeV.

As demonstrated in Böttcher & Dermer (2005),  $\gamma Z$  absorption in the stellar wind of the companion as well as  $\gamma\gamma$  absorption on star light photons reprocessed in the stellar wind are negligible compared to the direct  $\gamma\gamma$  absorption effect for LS 5039.

Consequently, the only relevant effect modifying the VHE  $\gamma$ -ray spectrum of LS 5039 at energies above  $\sim 100$  GeV between the emission site and the observer on Earth is  $\gamma\gamma$  absorption by direct star light photons. This effect can easily be corrected for by multiplying the observed spectra by a factor  $e^{\tau_{\gamma\gamma}(E)}$ , where  $\tau_{\gamma\gamma}(E)$  is the  $\gamma\gamma$  absorption depth along the line of sight.

#### 4. Deabsorbed VHE $\gamma$ -ray spectra

In this section, we present a parameter study of the deabsorbed photon spectra and integrated VHE  $\gamma$ -ray fluxes for representative of the viewing angle of  $i = 20^\circ, 40^\circ$ , and  $60^\circ$  and a range of locations of the emission site, characterized by a height  $z_0$  above the compact object in the direction perpendicular to the orbital plane. The absorption depth  $\tau_{\gamma\gamma}(E)$  along the line of sight is evaluated as described in detail in Böttcher & Dermer (2005). The observed spectra are represented by the best-fit functional forms quoted in the introduction.

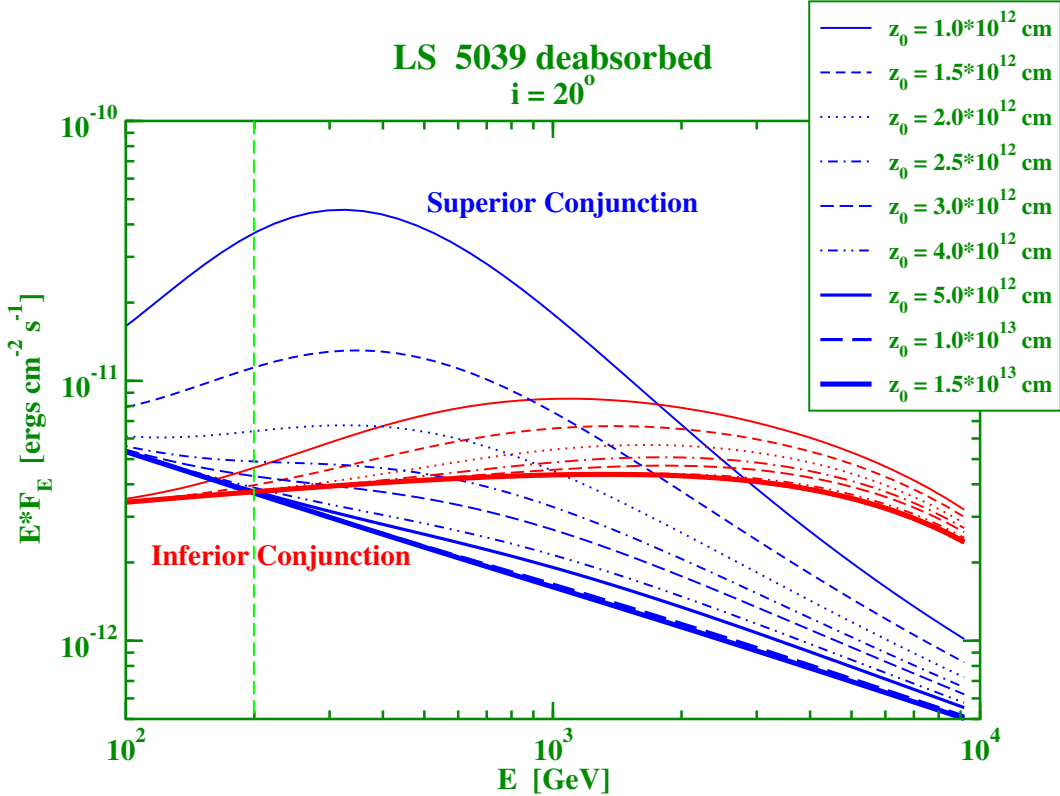


Fig. 2.— Deabsorbed VHE  $\gamma$ -ray spectra of LS 5039 for  $i = 20^\circ$  and a range of heights of  $z_0$  of the emission region above the compact object. The vertical dashed line indicates the energy threshold of the MAGIC observations.

Figures 2 — 4 show the inferred intrinsic, deabsorbed VHE  $\gamma$ -ray spectra from LS 5039 for a range of  $10^{12} \text{ cm} \leq z_0 \leq 1.5 \times 10^{13} \text{ cm}$ . At larger distances from the compact object,  $\gamma\gamma$  absorption due to the stellar radiation field becomes negligible for all inclination angles. Furthermore, models which assume a distance greatly in excess of the characteristic orbital separation (i.e.,  $z_0 \gtrsim 10^{13} \text{ cm}$ ) may be hard to reconcile with the periodic modulation of the emission on the orbital time scale. As the height  $z_0$  approaches values of the order of the characteristic orbital separation,  $s \sim 2 \times 10^{12} \text{ cm}$ , the intrinsic spectra would have to exhibit a significant excess towards the threshold of the MAGIC observations at  $E_{\text{thr}} \sim 200 \text{ GeV}$  in order to compensate for the  $\gamma\gamma$  absorption trough with its extremum around  $\sim 300 \text{ GeV}$  (Böttcher & Dermer 2005). At even smaller distances from the compact object,  $z_0 \ll 10^{12} \text{ cm}$ , the absorption features would again become essentially independent of  $z_0$  since the overall geometry would not change significantly anymore with a change of  $z_0$ .

A first, important conclusion from Figures 2 — 4 is that there is no combination of  $i$

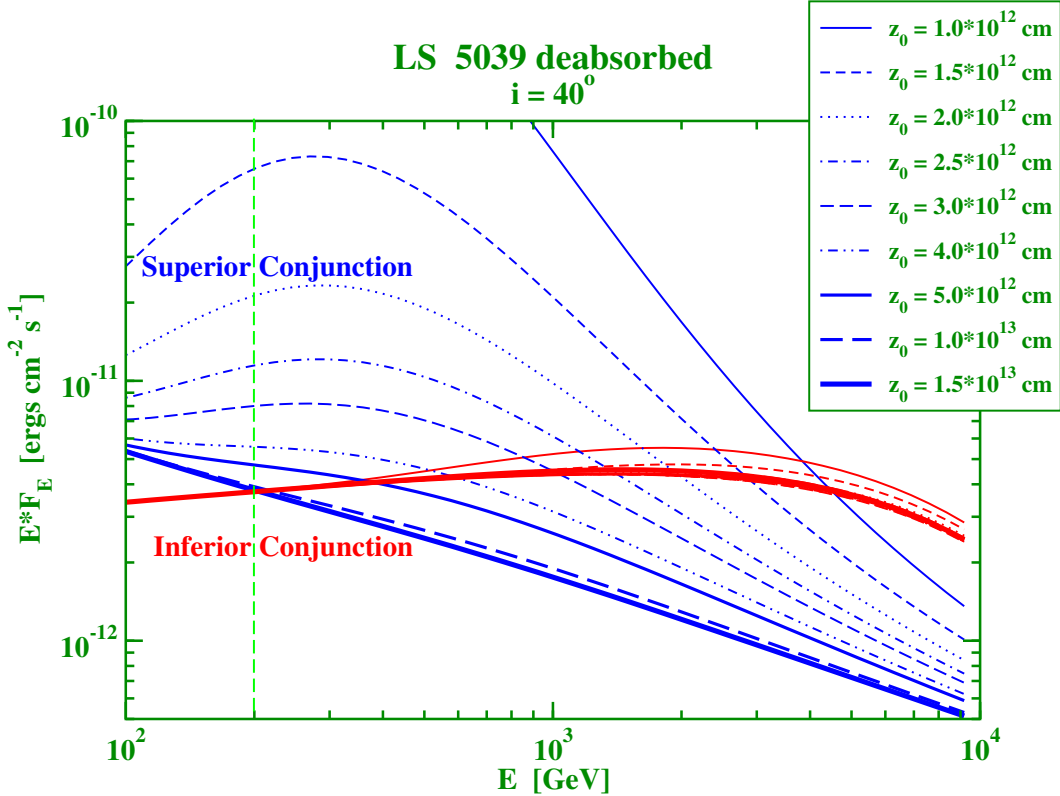


Fig. 3.— Deabsorbed VHE  $\gamma$ -ray spectra of LS 5039 for  $i = 40^\circ$  and a range of heights  $z_0$  of the emission region above the compact object. The vertical dashed line indicates the energy threshold of the MAGIC observations.

and  $z_0$  for which the de-absorbed VHE  $\gamma$ -ray spectra in the inferior and superior conjunction could be identical. Thus, the intrinsic VHE  $\gamma$ -ray spectra must be fundamentally different in the different orbital phases corresponding to superior conjunction (near periastron) and inferior conjunction (closer to apastron).

Second, there is a large range of instances in which the deabsorbed, differential photon fluxes at  $200 \text{ GeV} \lesssim E \lesssim 10 \text{ TeV}$  during superior conjunction would have to be substantially higher than during inferior conjunction, opposite to the observed trend. This could have interesting consequences for strategies of searches for high-energy neutrinos. To a first approximation, the intrinsic, unabsorbed VHE  $\gamma$ -ray flux is roughly equal to the expected high-energy neutrino flux (see, e.g., Lipari 2006). Therefore, our results suggest that phases with lower observed VHE  $\gamma$ -ray fluxes from LS 5039 may actually coincide with phases of larger neutrino fluxes. This is confirmed by a plot of the integrated  $0.2 - 10 \text{ TeV}$  photon fluxes as a function of height of the emission region as shown in Figure 5.

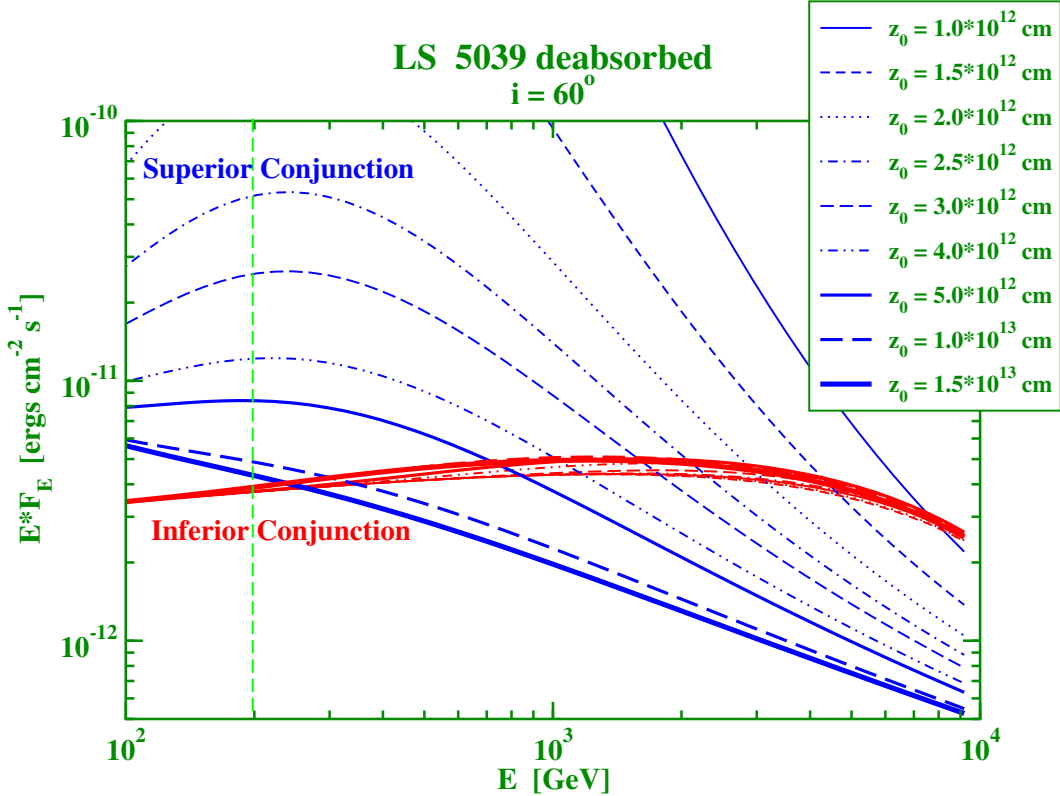


Fig. 4.— Deabsorbed VHE  $\gamma$ -ray spectra of LS 5039 for  $i = 60^\circ$  and a range of heights  $z_0$  of the emission region above the compact object. The vertical dashed line indicates the energy threshold of the MAGIC observations.

However, high-energy neutrino detectors such as AMANDA, IceCube, or ANTARES have much higher effective low-energy detection thresholds than MAGIC (typically 1 TeV or higher). Thus, a more realistic comparison should be based on the expected  $> 1$  TeV fluxes for the various geometrical scenarios investigated here. Their dependence on  $i$  and  $z_0$  is plotted in Figure 6 which indicates that there is actually a much more restricted range of configurations for which the neutrino flux in superior conjunction would exceed the one at inferior conjunction. Specifically, this would require emission region heights of  $z_0 \lesssim 10^{12}$  cm ( $i = 20^\circ$ ),  $2 \times 10^{12}$  cm ( $i = 40^\circ$ ), and  $3 \times 10^{12}$  cm ( $i = 60^\circ$ ), respectively. As we will see in the next section, for  $i i = 40^\circ$  and  $i = 60^\circ$ , these configurations can be ruled out because of constraints on the available power from wind accretion onto the compact object.

### Integrated, deabsorbed fluxes for LS 5039

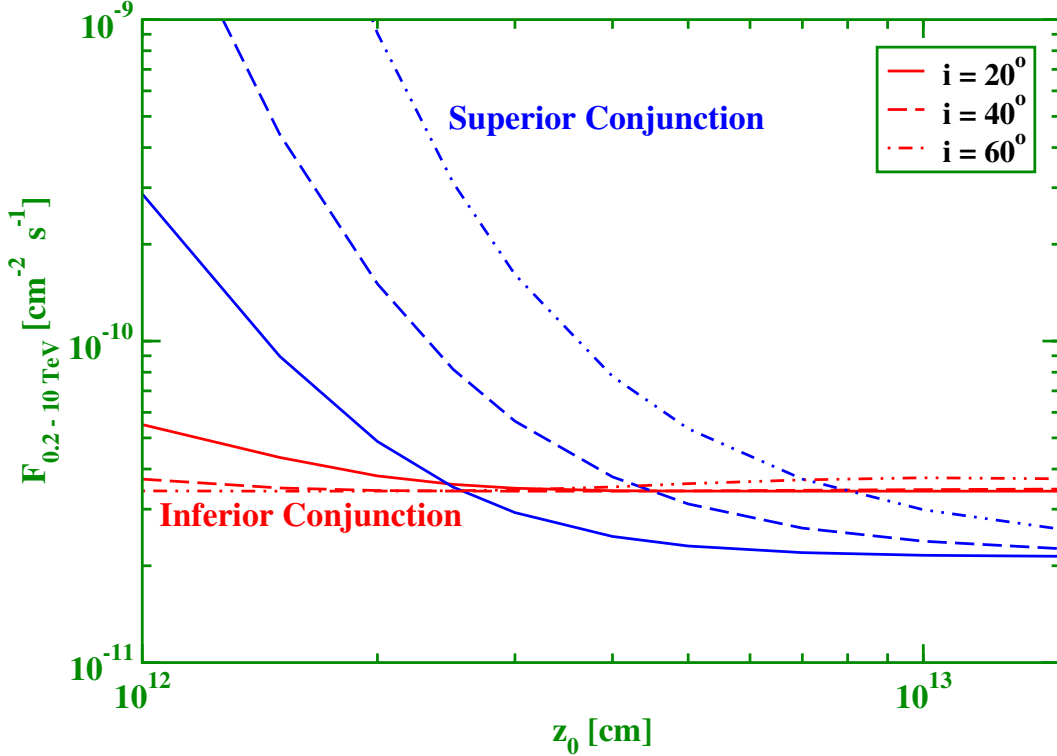


Fig. 5.— Deabsorbed, integrated 0.2 – 10 TeV  $\gamma$ -ray fluxes of LS 5039 as a function of height  $z_0$  of the emission region above the compact object. These numbers would also approximately equal to the expected neutrino fluxes in the same energy range.

### 5. Constraints from Accretion Power Limits

The inferred intrinsic (deabsorbed) VHE  $\gamma$ -ray fluxes calculated in the previous section imply apparent isotropic 0.1 – 10 TeV luminosities in the range of  $\sim 2 \times 10^{34} - 7 \times 10^{34}$  ergs/s ( $i = 20^\circ$ ),  $\sim 1.3 \times 10^{34} - 7 \times 10^{35}$  ergs/s ( $i = 40^\circ$ ), and  $\sim 1.2 \times 10^{34} - \gg 10^{37}$  ergs/s ( $i = 60^\circ$ ), respectively, for emission regions located at  $z_0 \geq 10^{12}$  cm (see Figure 7). These should be confronted with constraints on the available power from wind accretion from the stellar companion onto the compact object.

For this purpose, we assume that for a given directed wind velocity of  $v_{\text{wind}} \approx 2.5 \times 10^8$  cm/s, all matter with  $(1/2)v_{\text{wind}}^2 < GM_{\text{c.o.}}/R_{\text{BH}}$  will be accreted onto the compact object. An absolute maximum on the available power is then set by  $L_{\text{max}} \approx (1/12)\dot{M}_{\text{wind}} c^2 (R_{\text{BH}}^2/[4s^2])$ . We furthermore allow for Doppler boosting of this accretion power along the microquasar jet with the Doppler boosting factors  $D$  listed in Table 1. This

### Integrated, deabsorbed fluxes for LS 5039

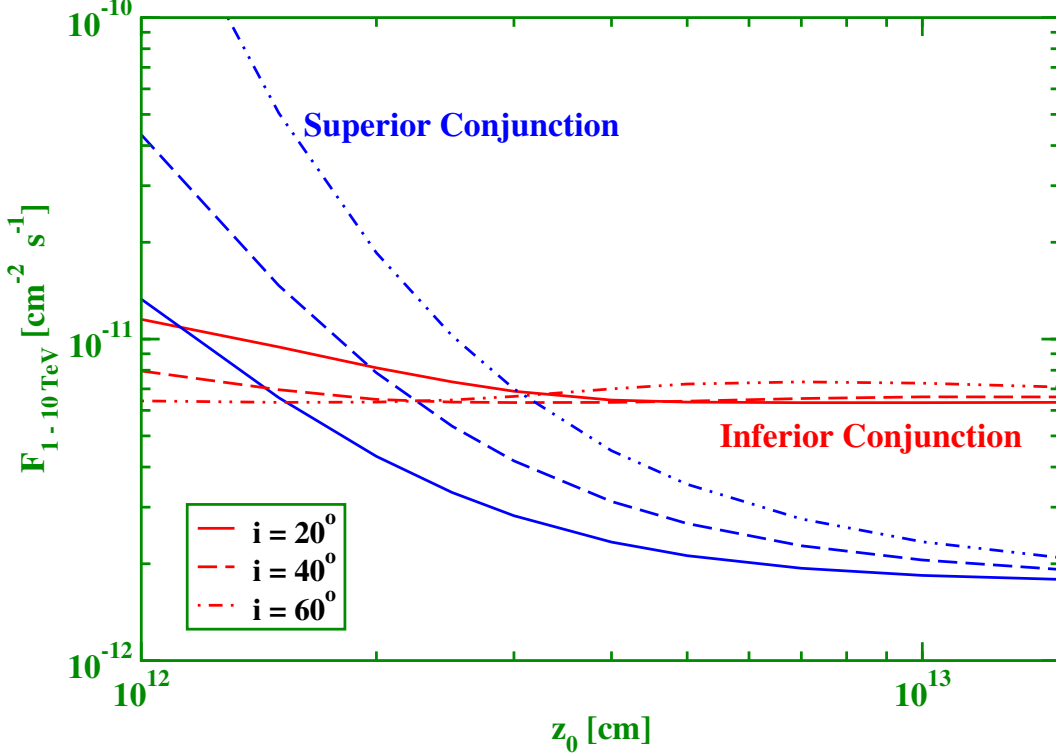


Fig. 6.— Deabsorbed, integrated  $1 - 10$  TeV  $\gamma$ -ray fluxes of LS 5039 as a function of height  $z_0$  of the emission region above the compact object. These numbers would also approximately equal to the expected neutrino fluxes in the same energy range.

yields an available power corresponding to an inferred, apparent isotropic luminosity of

$$L_{\max}^{\text{iso}} \approx 2.8 \times 10^{33} \left( \frac{M_{\text{c.o.}}}{M_{\odot}} \right)^2 D^4 \left( \frac{s}{2 \times 10^{12} \text{ cm}} \right)^{-2} \left( \frac{v_{\text{wind}}}{2.5 \times 10^8 \text{ cm/s}} \right)^{-4} \text{ ergs/s.} \quad (1)$$

The resulting luminosity limits are also included in Table 1 and indicated by the horizontal lines in Figure 7, where the respective higher value of the limit corresponds to  $\Gamma = 2$  and the lower value corresponds to  $\Gamma = 1.02$  for  $i = 20^\circ$  and  $40^\circ$ . For  $i = 60^\circ$ , the ordering is opposite because the emission would actually be de-boosted ( $D < 1$ ) for  $\Gamma = 2$  and  $i = 60^\circ$ . Allowed configurations are those for which the inferred, apparent isotropic  $0.1 - 10$  TeV luminosity is substantially below the respective luminosity limit. The resulting limits on the height  $z_0$  are summarized in Table 2

The figure indicates that for  $i = 20^\circ$ , virtually all configurations are allowed, even if the

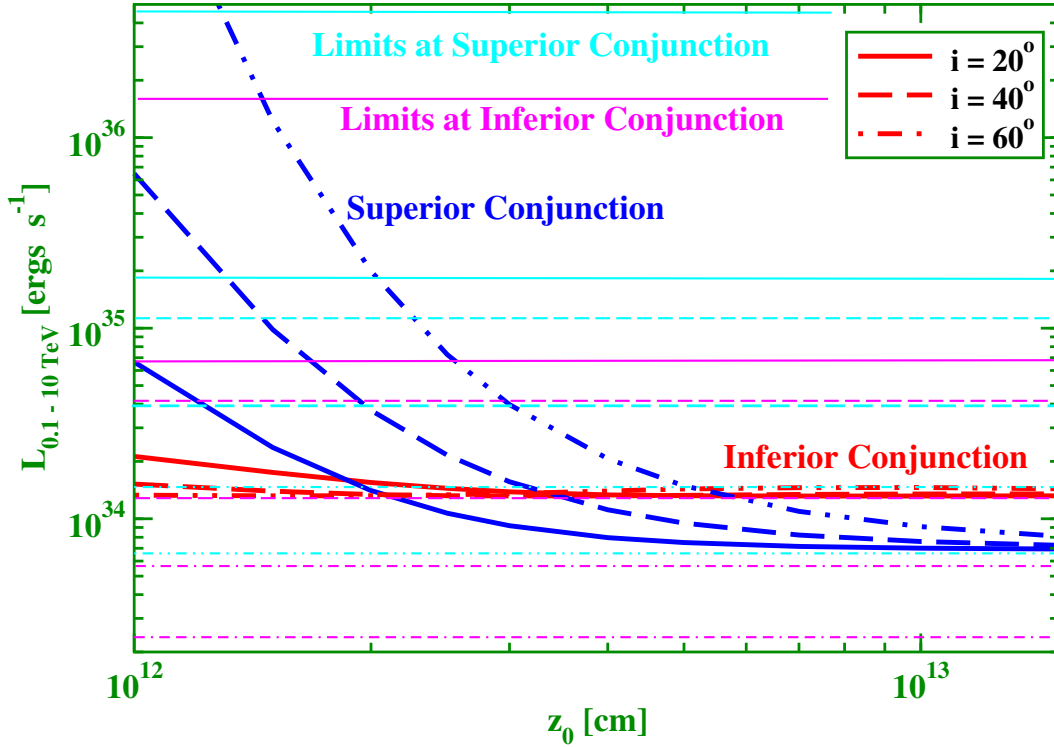


Fig. 7.— Inferred apparent isotropic luminosities for LS 5039 (thick curves), compared to the luminosity limits from Bondi-Hoyle limited wind accretion (horizontal lines). For  $i = 20^\circ$  and  $i = 40^\circ$ , the higher limits correspond to  $\Gamma = 2$ , the lower values of the upper limits correspond to  $\Gamma = 1.2$ . For  $i = 60^\circ$ , the ordering is opposite because the source would be de-boosted at  $\Gamma = 2$  and  $i = 60^\circ$ . Allowed configurations are those for which the inferred luminosities are substantially below the

emission is essentially unboosted ( $\Gamma = 1.02$ ) and originates very close to the compact object.

For  $i = 40^\circ$  at the time of superior conjunction, one can set a limit of  $z_0 \gtrsim 2 \times 10^{12}$  cm. For this viewing angle, the limit implied for  $\Gamma = 1.02$  is always below the inferred value, indicating that this configuration is ruled out. This implies that, if  $i \sim 40^\circ$ , the emission at the time of inferior conjunction must be substantially Doppler enhanced.

The situation is even more extreme for  $i = 60^\circ$ . Under this viewing angle, only the  $\Gamma = 1.02$  scenario leads to an allowed model and requires  $z_0 \gtrsim 5 \times 10^{12}$  cm. Since there is no allowed scenario to produce the observed flux at inferior conjunction, one can conclude that a large inclination angle of  $i \sim 60^\circ$  may be ruled out.

## 6. Summary and Discussion

In this paper, a detailed study of the intrinsic VHE  $\gamma$ -ray emission from the Galactic microquasar LS 5039 after correction for  $\gamma\gamma$  absorption by star light photons from the massive companion star is presented. This system had shown evidence for an orbital modulation of the VHE  $\gamma$ -ray flux and spectral shape. A range of observationally allowed inclination angles,  $13^\circ \leq i \leq 64^\circ$  (specifically,  $i = 20^\circ$ ,  $i = 40^\circ$ , and  $i = 60^\circ$ ) as well as plausible distances  $z_0$  of the VHE  $\gamma$ -ray emission region above the compact object ( $10^{12} \text{ cm} \leq z_0 \leq 1.5 \times 10^{13} \text{ cm}$ ) was explored. Deabsorbed, intrinsic VHE  $\gamma$ -ray spectra as well as integrated fluxes and inferred, apparent isotropic luminosities were calculated and contrasted with constraints from the available power from wind accretion from the massive companion onto the compact object. The main results are:

- It is impossible to choose the viewing angle and location of the VHE emission region in a way that the intrinsic (deabsorbed) fluxes and spectra in superior and inferior conjunction are identical within the range of values of  $i$  and  $z_0$  considered here. For values of  $z_0$  much smaller and much larger than the characteristic orbital separation ( $s \sim 2 \times 10^{12} \text{ cm}$ ), the absorption features would become virtually independent of  $z_0$ . Furthermore, models assuming a VHE  $\gamma$ -ray emission site at a distance greatly in excess of the orbital separation might be difficult to reconcile with the orbital modulation of the VHE emission. Consequently, the intrinsic VHE luminosities and spectral shapes must be fundamentally different in different orbital phases.
- It was found that the luminosity constraints for an inclination angle of  $i = 60^\circ$  at inferior conjunction could not be satisfied at all, and for  $i = 40^\circ$ , there is no allowed configuration in agreement with the luminosity constraint for  $\Gamma = 1.02$ . From this, it may be concluded that, if the VHE luminosity is limited by wind accretion from the companion star and the system is viewed at an inclination angle of  $i \gtrsim 40^\circ$ , the emission is most likely beamed by a larger Doppler factor than inferred from the dynamics of the large-scale radio outflows on scales of several hundred AU.
- Since it was found to be impossible to satisfy the luminosity constraint for inferior conjunction at a viewing angle of  $i = 60^\circ$ , one can constrain the viewing angle to values substantially smaller than the maximum of  $\sim 64^\circ$  inferred from the lack of eclipses.
- The previous two points as well as the fact that the luminosity limits can easily be satisfied for  $i = 20^\circ$ , indicate that a rather small inclination angle  $i \sim 20^\circ$  may be preferred. Thus, our results confirm the conjecture of Casares et al. (2005) that the compact object might be a black hole rather than a neutron star.

- Comparing the ranges of allowed configurations from Table 2 to the plot of intrinsic  $> 1$  TeV fluxes in Figure 6, one can see that there is a limited range of allowed configurations for which the expected  $> 1$  TeV neutrino flux would actually anti-correlate with the observed VHE  $\gamma$ -ray emission. Specifically, for a preferred viewing angle of  $i \sim 20^\circ$ , models in which the emission originates within  $z_0 \lesssim 10^{12}$  cm would predict that the  $> 1$  TeV neutrino flux at superior conjunction is larger than at inferior conjunction, opposite to the orbital modulation trend seen in VHE  $\gamma$ -ray photons. Thus, strategies for the identification of high-energy neutrinos from microquasars based on a positive correlation with observed VHE fluxes may fail if models with  $z_0 \lesssim 10^{12}$  cm apply.

The author thanks F. Aharonian and V. Bosch-Ramon for stimulating discussions and hospitality during a visit at the Max-Planck-Institute for Nuclear Physics, and M. De Naurois for providing the HESS data points. This work was partially supported by NASA INTEGRAL Theory grant no. NNG 05GK59G and a scholarship at the Max-Planck Institute for Nuclear Physics in Heidelberg.

## REFERENCES

Aharonian, F. A., et al., 2005, *Science*, 309, 746

Aharonian, F. A., et al., 2006, *A&A*, submitted (astro-ph/0607192)

Albert, J., et al., 2006, *Science*, vol. 312, issue 5781, p. 1771

Bednarek, W., 1997, *A&A*, 322, 523

Bednarek, W., 2000, *A&A*, 362, 646

Böttcher, M., & Dermer, C. D., 2005, *ApJ*, 634, L81

Bosch-Ramon, V., & Paredes, J. M., 2004, *A&A*, 417, 1075

Bosch-Ramon, V., Romero, G. E., & Paredes, J. M., 2005a, *A&A*, 429, 267

Bosch-Ramon, V., Aharonian, F. A., & Paredes, J. M., 2005b, *A&A*, 432, 609

Casares, J., Ribó, M., Ribas, I., Paredes, J. M., Martí, J., & Herrero, A., 2005, *MNRAS*, 364, 899

Chernyakova, M., Neronov, A., & Walter, R., 2006, MNRAS, submitted (astro-ph/0606070)

Dermer, C. D., & Böttcher, M., 2006, ApJ, 643, 1081

Gregory, P. C., 2002, ApJ, 575, 427

Dubus, G., 2006a, A&A, 451, 9

Dubus, G., 2006b, A&A, submitted (astro-ph/0605287)

Gregory, P. C., & Taylor, A. R., 1978, Nature, 272, 704

Gupta, S., Böttcher, M., & Dermer, C. D., 2006, ApJ, 644, 409

Gupta, S., & Böttcher, M., 2006, ApJ, submitted (astro-ph/0606590)

Kniffen, D. A., et al. 1997, ApJ, 486, 126

Lipari, P., in proc. of “Very Large Volume Neutrino Telescopes”, Catania, Italy, 2005, in press (astro-ph/0605535)

McSwain, M. V., & Gies, D. R., 2002, ApJ, 568, L27

Moskalenko, I. V., Karakula, S., & Tkaczyk, W., 1993, MNRAS, 260, 681

Moskalenko, I. V., & Karakula, S., 1994, ApJS, 92, 567

Paredes, J. M., Martí, J., Ribó, M., & Massi, M., 2000, Science, 288, 2340

Paredes, J. M., Ribó, M., Ros, E., Martí, J., & Massi, M., 2002, A&A, 393, L99

Reimer, A., Pohl, M., & Reimer, O., 2006, ApJ, 644, 1118

Romero, G. E., Torres, D. F., Kaufman Bernadó, M. M., & Mirabel, I. F., 2003, A&A, 410, L1

Taylor, A. R., Kenny, H. T. Spencer, R. E., & Tzioumis, A., 1992, ApJ, 395, 268

Table 2. Lower limits on the height of the VHE  $\gamma$ -ray emission site above the compact object inferred from Figure 7. Configurations for which the intrinsic apparent isotropic luminosity would always be larger than the available accretion power can not be realized and are marked as “forbidden”.

$i$ [°]	position	$z_0^{\min}(\Gamma = 1.02)$ [10 <sup>12</sup> cm]	$z_0^{\min}(\Gamma = 2)$ [10 <sup>12</sup> cm]
20	i.c.	$\ll 1$	$\ll 1$
20	s.c.	$\ll 1$	$\ll 1$
40	i.c.	forbidden	$\ll 1$
40	s.c.	2.0	1.5
60	i.c.	forbidden	forbidden
60	s.c.	5	forbidden